

## Rapid Communication

# Echo train shifted multi-echo FLASH for functional MRI of the human brain at ultra-high spatial resolution

Dirk Voit and Jens Frahm\*

Biomedizinische NMR Forschungs GmbH am Max-Planck-Institut für Biophysikalische Chemie, 37070 Göttingen, Germany

Received 6 July 2005; Revised 23 September 2005; Accepted 23 September 2005

**ABSTRACT:** This paper describes the development of a novel technique for functional MRI of the human brain at 0.135  $\mu\text{L}$  resolution for a whole brain section. In comparison with conventional studies at 3 mm isotropic resolution or 27  $\mu\text{L}$  voxel size, the method yields an improvement by a factor of 200. To achieve optimum image quality, the approach is based on a multi-echo fast low-angle shot (FLASH) sequence with unipolar traversals of  $k$ -space in the frequency-encoding dimension and echo train shifting to avoid amplitude discontinuities in the phase-encoding dimension. These strategies ensure a smooth point-spread function and eliminate image ghosting artifacts without the need for any phase correction or other post-processing. Signal-to-noise losses due to the considerably reduced voxel sizes are compensated for by single slice acquisitions, optimized bandwidths and an experimental four-channel shoulder coil matched to the posterior portion of the head. Multi-echo FLASH studies of the human brain (2.9 T, seven echoes, 200 Hz/pixel bandwidth, effective echo time 36 ms, acquisition time 6 s) at 300  $\mu\text{m}$  resolution (no interpolation) and 1.5 mm slice thickness revealed robust activations in primary visual areas in response to binocular stimulation. The new method holds promise for refined studies of the columnar organization of specific brain systems and for functional assessments of the gray matter at laminar resolution. Copyright © 2005 John Wiley & Sons, Ltd.

**KEYWORDS:** functional magnetic resonance imaging (fMRI); functional neuroimaging; human brain; spatial resolution; visual activation

## INTRODUCTION

Since the inception of functional MRI of human brain using blood oxygenation level dependent (BOLD) contrast (1), one of its specific advantages is access to very high spatial resolution. Technical approaches range from early single-echo fast low-angle shot FLASH MRI applications (2,3) at 1.5 and 2 T covering a whole brain section to more recent studies at 7 T which employed a segmented Hahn spin-echo echo-planar imaging (EPI) sequence and reached a nominal resolution of  $0.5 \times 0.5 \times 3 \text{ mm}^3$  although for only a limited field-of-view (FOV) (4). The potential for high-resolution studies is due to the microscopic nature of the deoxyhemoglobin-induced paramagnetic field perturbations and supported by physiological evidence that the regulation of the microvasculature in response to a functional challenge is tightly controlled in terms of spatial accuracy. Of course, imaging at very high spatial resolution does not necessarily reflect an equivalent

spatial accuracy of the BOLD MRI-detected neural response if the BOLD effect itself becomes 'smeared' by the local hemodynamic properties. However, to address these issues, a high-quality imaging sequence is needed in the first place.

While assessments of experimental animals obviously require an adequate resolution to monitor BOLD MRI responses in small brains, high-resolution studies of humans complement the mainstream of applications at lower resolution which focus on mapping cortical and subcortical networks *across* brain systems by a more detailed delineation of the functional organization *within* a particular system or cortical unit. The most prominent example is the structural analysis of information processing in the primary visual cortex which occurs in a pattern of spatially alternating cortical columns for the left and right eye with a surface diameter of about 0.5–1 mm. Previous work addressed such questions with a typical in-plane resolution of  $0.5 \times 0.5 \text{ mm}^2$  and a section thickness of 3–4 mm using FLASH (5,6) or segmented EPI (7–10).

The purpose of this work was to develop an experimental strategy that specifically matches the requirements for a further refinement of functional MRI studies at very high spatial resolution. A key to this problem is an MRI sequence with optimum image quality

\*Correspondence to: J. Frahm, Biomedizinische NMR Forschungs GmbH, 37070 Göttingen, Germany.  
E-mail: jfracm@gwdg.de

**Abbreviations used:** BOLD, blood oxygenation level dependent; CHES, chemical shift selective; EPI, echo-planar imaging; FLASH, fast low-angle shot; FOV, field-of-view; GRASE, gradient-echo and spin-echo; RF, radiofrequency; SNR, signal-to-noise ratio.

that achieves the desired resolution without potentially critical post-processing corrections and by using 'true' acquisitions, that is, without zero filling or other interpolation techniques. The approach chosen here attempts to take the best of both FLASH and EPI and therefore emerges as a multi-echo FLASH sequence with unipolar traversals of  $k$ -space rather than segmented EPI.

## MATERIALS AND METHODS

### Multi-echo FLASH sequence

A generic multi-echo FLASH sequence is shown in Fig. 1 for the case of three gradient echoes per  $TR$ . The sequence acquires unipolar lines in  $k$ -space that are equally spaced apart and therefore in this case subdivide the  $k$ -space in three equal parts. The lower part of Fig. 1 demonstrates the actual trajectory for this version. Accordingly, the phase-encoding gradient comprises an initial variable dephasing part before the generation of the first frequency-encoding

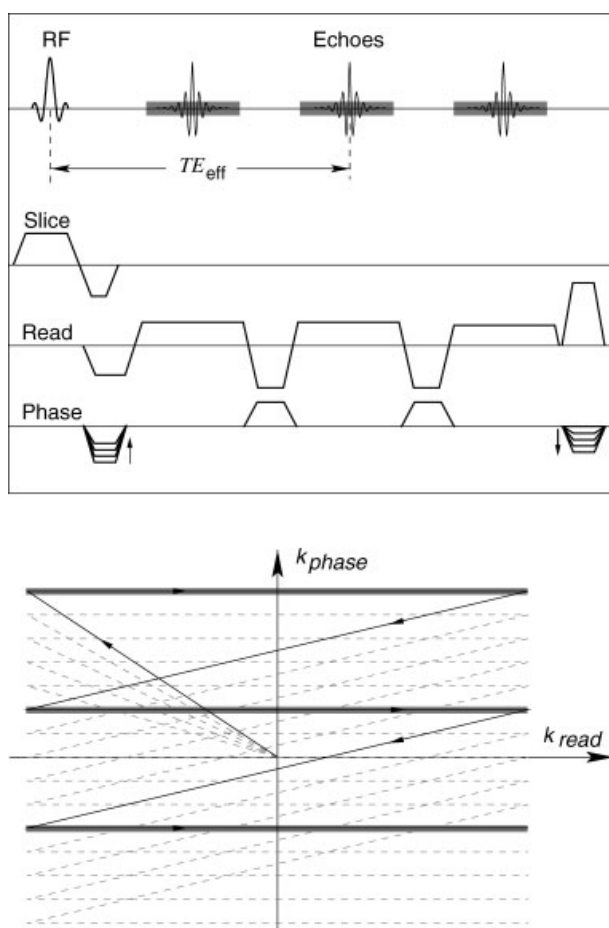


**Figure 1.** Top: multi-echo FLASH sequence (here: three echoes, effective echo time  $TE_{eff}$ ) including a phase-encoding rewinder for constant phase per  $TR$  and a spoiler gradient in readout direction. Bottom: corresponding  $k$ -space traversal

gradient echo and constant rephasing gradients before subsequent echoes. The effective echo time  $TE_{eff}$  refers to the echo time of the middle echo covering the central portion of  $k$ -space. To facilitate radiofrequency (RF) spoiling for pure  $T_2^*$ -weighted spin density (or  $T_1$ ) contrast, residual phase information is rephased by a final rewinding gradient at the end of  $TR$  in order to keep the net phase constant in every  $TR$  interval, that is, at the value obtained for the first echo train. The additional spoiler gradient in the frequency-encoding direction further eliminates inter- $TR$  and inter-image signal fluctuations in repetitive applications.

Because gradient-echo sequences with multiple echo times are sensitive to off-resonance effects such as the water–fat chemical shift difference, this problem was taken care of by a preceding fat saturation module. It represents a chemical shift selective (CHESS) pulse with its carrier frequency centered on the fat resonance (about 1.2 ppm) followed by a sufficiently strong spoiler gradient. For applications to the human brain with a section thickness of  $\geq 1.5$  mm as shown here, RF excitation was accomplished with a conventional slice-selective low-flip angle pulse characterized by a sinc shape, a pulse duration of 2.56 ms, 512 support points and a bandwidth–time product of 2.68. Additional improvements of the slice profile may be achieved by prolonging the pulse duration.

### Echo train shifting

When applied as shown in Fig. 1, multi-echo FLASH images suffer from ghosting artifacts that increase with increasing number of gradient echoes per  $TR$ . This is demonstrated for a high-resolution structural water phantom in the top row of Fig. 2 for sequences using three, five and seven echoes. The physical reason is due to the fact that the corresponding partitioning of  $k$ -space is accompanied by intensity discontinuities that reflect the different signal strengths of the gradient echoes at different echo times. Thus, in contrast to the even more pronounced but continuous  $T_2^*$  weighting of an EPI echo train, the  $k$ -space data of a multi-echo FLASH sequence contain 'jumps' which – after Fourier transformation – translate into ringing artifacts. In other words, the convolution of the echo train decay with multiple rectangles causes a multiplication of the point-spread function with corresponding sinc functions.

In order to overcome this obstacle, the sequence was combined with the principle of echo train shifting originally proposed by Feinberg and Oshio for the elimination of phase errors in gradient-echo and spin-echo (GRASE) sequences (11). As outlined in Fig. 3, the idea is to increment the echo times for successive Fourier lines of a particular  $k$ -space segment (or echo group) such that the signal intensity of the last echo approaches that of the first echo from the following segment. In practice, this temporal shift ( $dt$  in Fig. 3) is simply given by the echo

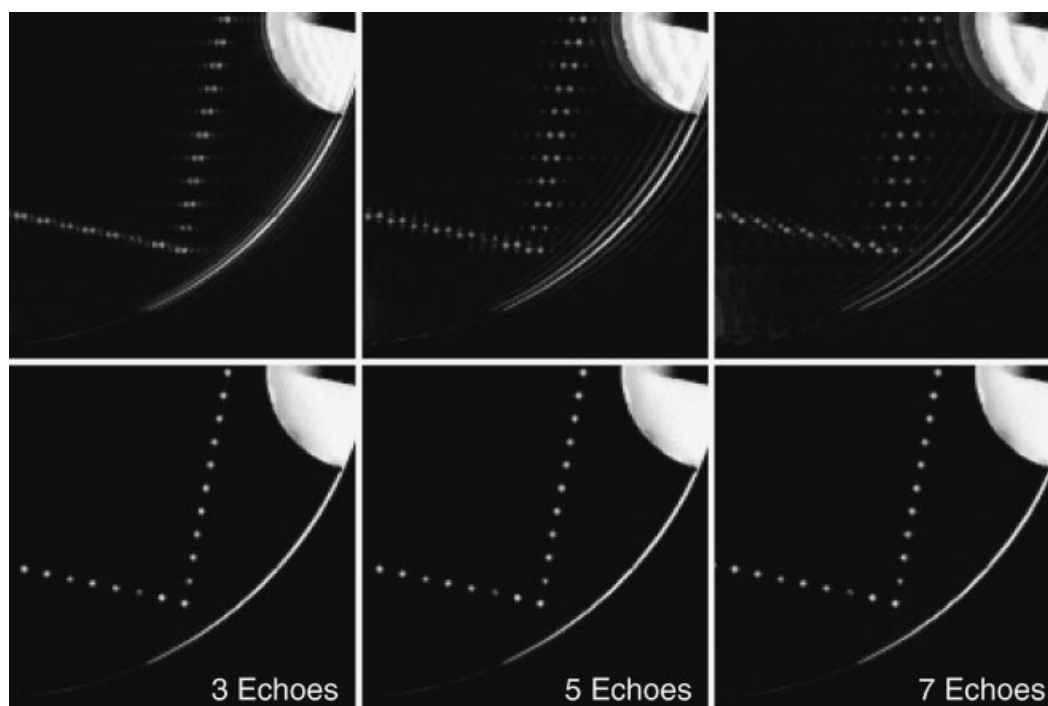


**Figure 2.** Multi-echo FLASH images of a high-resolution structural water phantom obtained (top) without and (bottom) with echo train shifting for the simultaneous acquisition of three, five and seven echoes at  $0.5 \times 0.5$  mm resolution and 4 mm section thickness (other parameters as in Table 1)

spacing divided by the number of RF excitations required which in turn is the number of phase-encoding steps divided by the number of  $k$ -space segments. The time shift is most easily applied to all echoes simultaneously, that is, to the complete echo train.

For the example shown in Figs 1 and 3, this strategy no longer results in three echo groups with three fixed echo times and correspondingly different signal amplitudes, but a smooth  $T_2^*$  decay for all Fourier lines which links the signal attenuation within the central part of  $k$ -space to that of the first and third echo groups. The bottom row of Fig. 2 clearly demonstrates the successful elimination of the ghosting artifacts after the implementation of echo train shifting for multi-echo FLASH. The procedure works for all echo numbers including echo trains with an even number of echoes (not shown). Moreover, the achieved image quality is obtained without the need for any post-processing. In particular, the sequence does not require the correction of phase errors such as are necessary, for example, for segmented EPI.

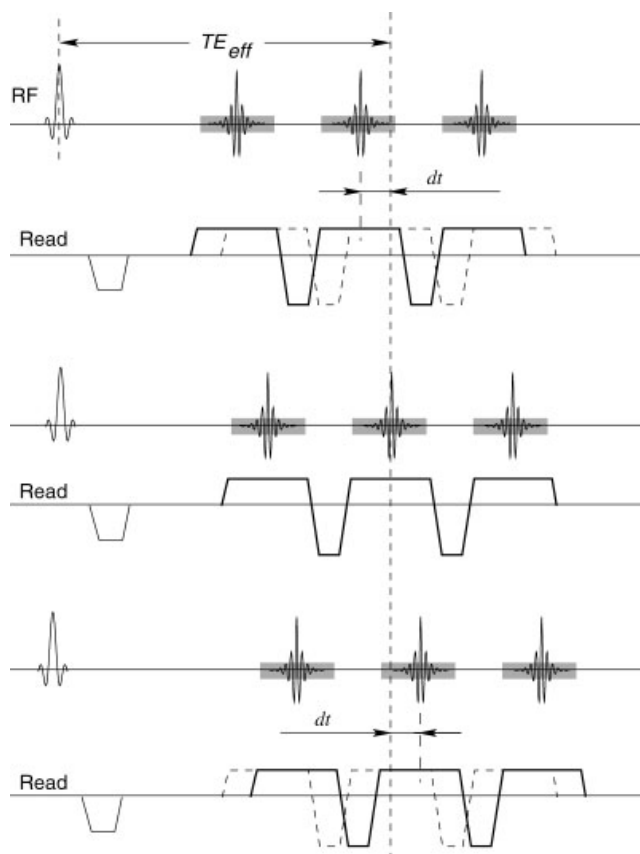
### Functional MRI of human brain

Table 1 summarizes the experimental parameters optimized for functional MRI of the human brain at different spatial resolutions. Although echo train shifted multi-echo FLASH sequences allow for an arbitrary numbers of echoes, the present studies were performed with seven echoes. Based on an effective echo time of  $TE = 36$  ms (at

3 T) and a potentially usable acquisition window of about 50 ms, the corresponding receiver bandwidths were chosen as small as possible to gain signal-to-noise ratio (SNR) and as high as necessary to avoid pronounced  $T_2^*$  attenuation. Typically, the echo spacing was about 8–8.5 ms for all resolutions, whereas the echo time shift  $dt$  decreased with increasing resolution from 0.78 to 0.12 ms because of the larger number of RF excitations.

An in-plane resolution of  $2 \times 2$  mm<sup>2</sup> was only implemented to compare the multi-echo FLASH results with single-shot gradient-echo EPI ( $TR/TE = 2000/36$  ms, flip angle  $70^\circ$ , frequency-selective fat suppression) in order to ensure consistency with routine methods at low resolution. Studies at intermediate high resolution, that is at  $1 \times 1$  and  $0.5 \times 0.5$  mm<sup>2</sup>, are currently being performed to detail the functional organization of the sensorimotor cortex. The highest resolution achieved so far corresponds to  $0.3 \times 0.3$  mm<sup>2</sup> for a whole brain section of 1.5 mm thickness and it is planned to revisit human brain systems at columnar and laminar resolution.

All studies were conducted at 2.9 T (Magnetom Trio, Siemens, Erlangen, Germany) using an eight-channel receive-only phased array headcoil (phantom studies) or an experimental four-channel shoulder coil (human studies) in combination with a body coil for RF transmission. The small shoulder coil was mounted so as to match closely the posterior portion of a subject's head and yielded a further improvement in SNR. Taken together, about 50 subjects participated in the study, including trials at different developmental stages and spatial



**Figure 3.** Echo train shifting of the readout gradient of multi-echo FLASH sequences (here: three echoes, three different repetitions shown) avoids amplitude discontinuities along the phase-encoding dimension of  $k$ -space. The slotted curves in the top and bottom rows correspond to the unshifted gradient waveform of the central acquisition and serve as a reference for the temporal shift  $dt$

resolutions. More than 10 subjects underwent functional MRI investigations with the final multi-echo FLASH sequence at the highest resolution presented here. In all cases, informed written consent was obtained before each examination.

Functional activation was elicited using a passive visual stimulation task, which compared an alternating

black-and-white checkerboard (12 s) with a gray screen (18 or 20 s). A low flicker frequency of 0.5 Hz was used for all experiments and chosen to improve a subject's tolerance to measurement durations of up to 15 min as required for acquisitions at ultra-high resolution (corresponding to 30 cycles of stimulation and control). Subjects were instructed to fixate towards a red fixation cross in the center of the screen throughout the experiment. MRI-compatible liquid crystal display goggles (Resonance Technology, Northridge, CA, USA) were used to present visual stimuli (60 Hz refresh rate,  $1024 \times 768$  pixel resolution,  $22.5 \times 30^\circ$  visual field, virtual eye-to-screen distance about 120 cm). Corrective lenses were applied if necessary.

Activation maps were calculated by a correlation analysis using a boxcar reference function which was derived from the task protocol but shifted by 4–6 s to account for the delayed hemodynamic response. Significant activations were identified by a statistical evaluation of correlation coefficients following a procedure described previously (12). Briefly, pixels are accepted as activated if their correlation coefficients exceed the 99.99% percentile rank of the noise distribution estimated on an individual basis from the actual measurement. In a second step, directly neighboring pixels are iteratively added as long as their correlation coefficients exceed the 95% percentile rank of the noise distribution. To account for statistical differences due to the very much larger number of image voxels at ultra-high resolution, the lower threshold was set to 85%. In all cases the resulting activation maps were superimposed on respective  $T_2^*$ -weighted raw images.

## RESULTS

Figures 4–6 summarize the results obtained for functional MRI of the human brain using echo train shifted multi-echo FLASH and visual stimulation. Figure 4 compares EPI (left) and multi-echo FLASH (right) at low resolution ( $2 \times 2 \text{ mm}^2$ ) and clearly demonstrates

**Table 1.** Echo train shifted multi-echo FLASH at different resolutions for a sequence comprising seven echoes (effective  $TE = 36 \text{ ms}$ ,  $FOV = 192 \times 144 \text{ mm}^2$ )

Parameter	Resolution (mm)			
	$2 \times 2$	$1 \times 1$	$0.5 \times 0.5$	$0.3 \times 0.3$
Repetition time (ms)	181.2	100	97.6	88.2
Acquisition time (s)	2	2	4	6
Bandwidth (Hz/pixel)	134	134	153	200
Flip angle ( $^\circ$ )	20	30	30	25
Matrix size	$96 \times 77$	$192 \times 140$	$384 \times 287$	$640 \times 476$
Echo spacing (ms)	8.09	8.53	8.52	8.24
Echo shift (ms)	0.73	0.42	0.20	0.12
Stimulus – control (s)	12–18	12–18	12–20	12–18
Number of cycles	6	12	16	30
Measuring time (min)	3	6	8	15

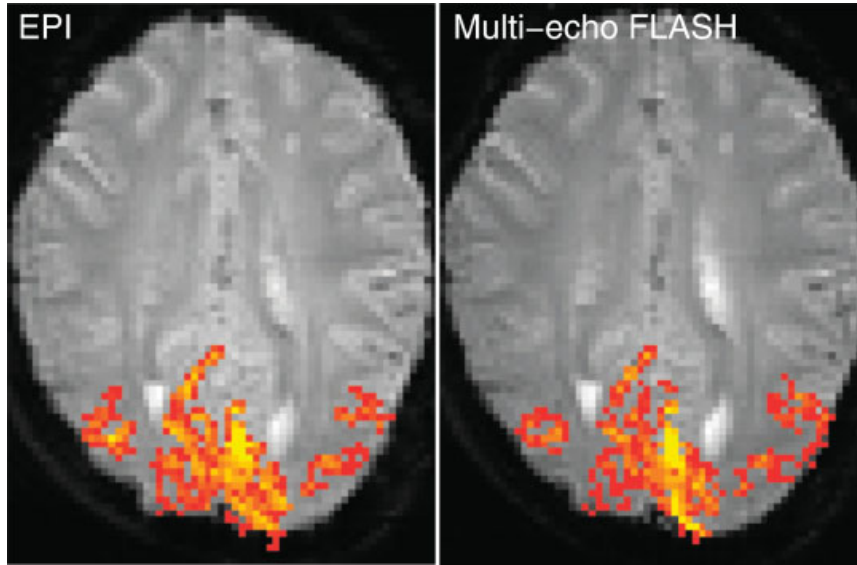


**Figure 4.** Low-resolution activation maps of the human brain for binocular visual stimulation using (left) EPI and (right) echo train shifted multi-echo FLASH at  $2 \times 2 \text{ mm}^2$  resolution and 4 mm section thickness (other parameters as in Table 1)

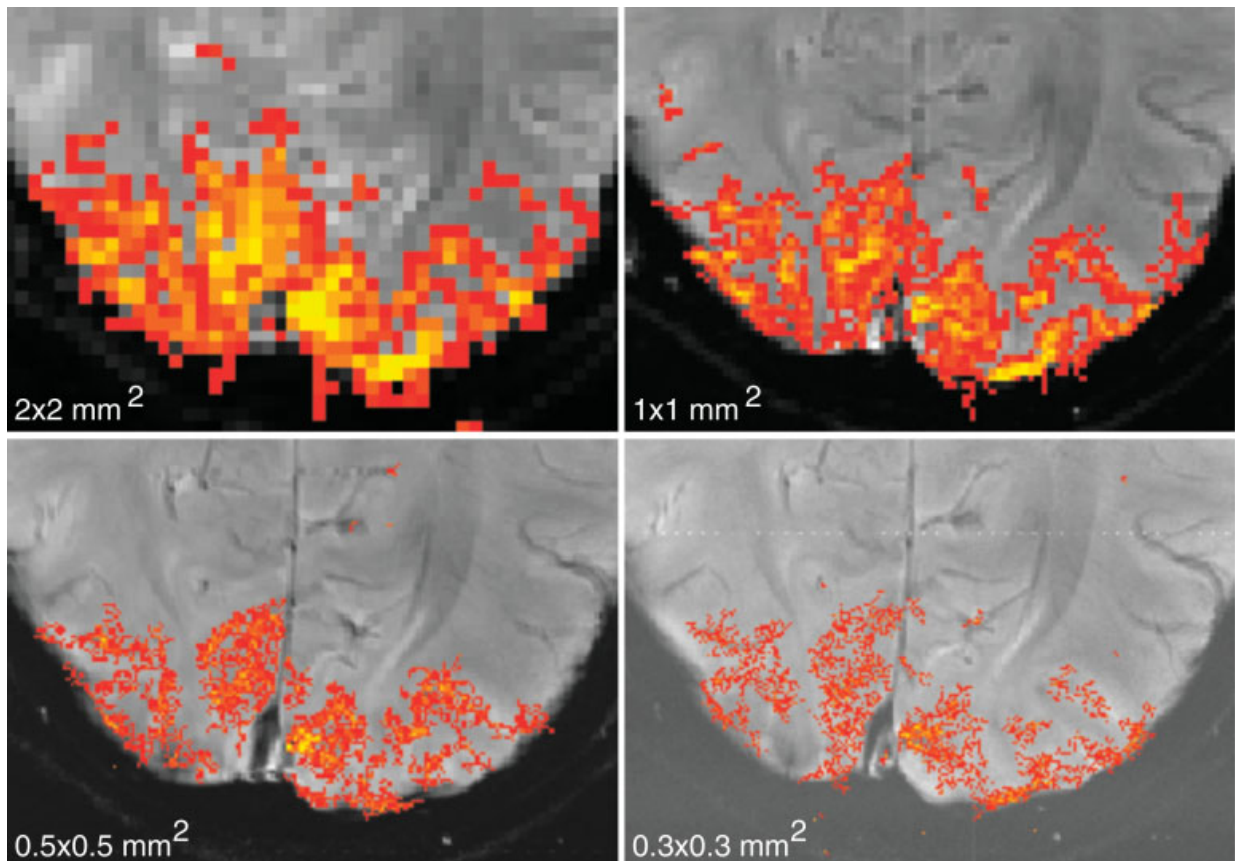


**Figure 5.** Activation maps of the human brain (different subject to Fig. 4) for binocular visual stimulation using echo train shifted multi-echo FLASH at  $2 \times 2$ ,  $1 \times 1$ ,  $0.5 \times 0.5$  and  $0.3 \times 0.3 \text{ mm}^2$  resolution and 4 mm section thickness (other parameters as in Table 1)

the consistency of the results in terms of spatial extent, functional contrast and statistical quality. In either case the statistical evaluation employed an upper threshold of 99.99% for activation foci and a lower threshold of

95% for accepting neighboring pixels as activated. Figure 5 shows activation maps of a different subject at different resolutions. The maps were obtained by using echo train shifted multi-echo FLASH at  $2 \times 2$ ,

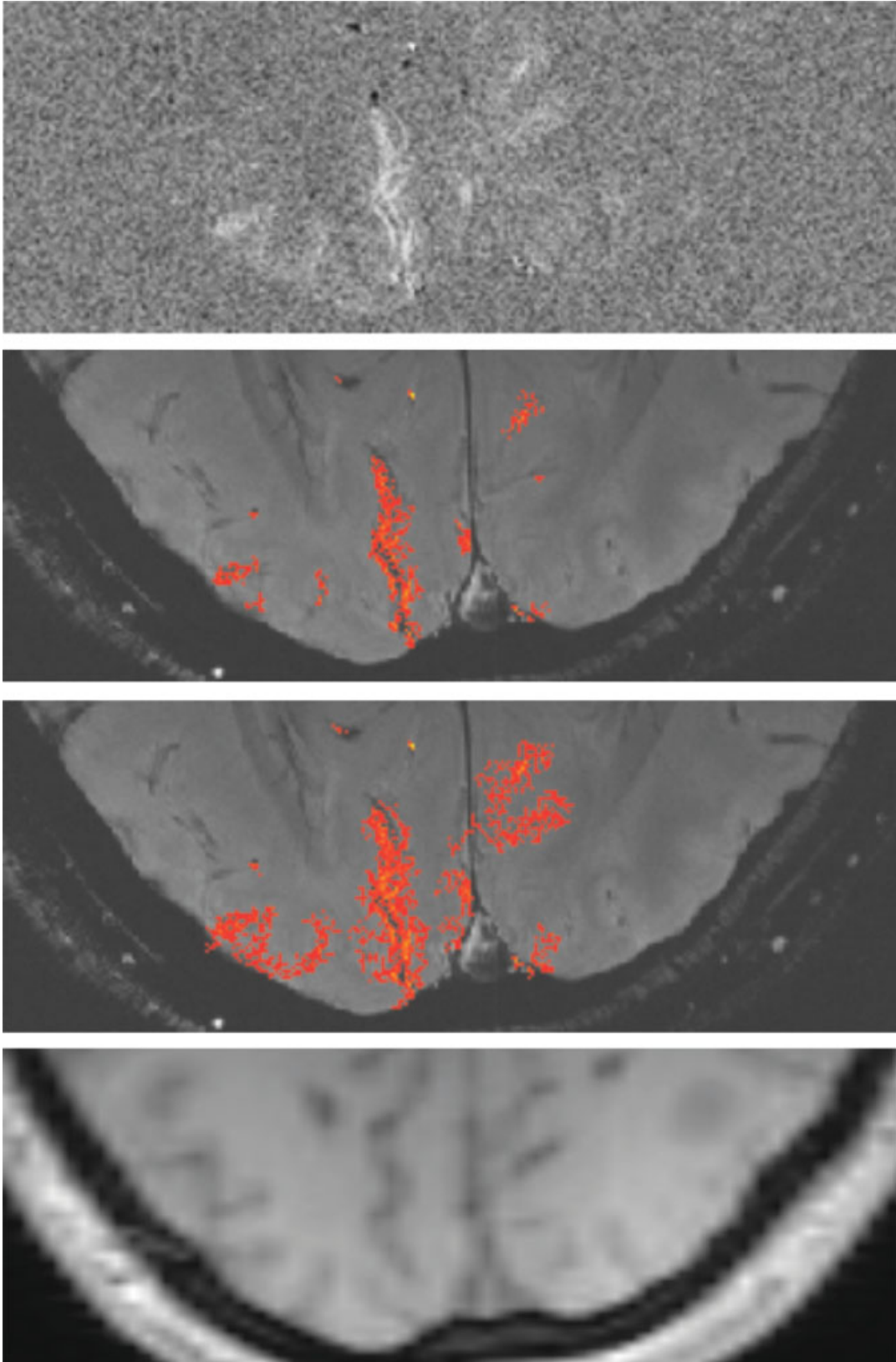


**Figure 6.** Ultra high-resolution activation maps of the human brain (different subject to Figs 4 and 5) for binocular visual stimulation using echo train shifted multi-echo FLASH at  $0.3 \times 0.3 \text{ mm}^2$  resolution and 1.5 mm section thickness (other parameters as in Table 1). Top: correlation coefficient map without any thresholding. Middle: statistically evaluated maps with an upper threshold of 99.99% and lower thresholds of 95 and 85% (for details see text) superimposed on an averaged raw image. Bottom: a  $T_1$ -weighted anatomical reference image at slightly lower resolution (3D spoiled FLASH)

$1 \times 1$ ,  $0.5 \times 0.5$  and  $0.3 \times 0.3$  mm<sup>2</sup> resolution and 4 mm section thickness. For the high-resolution studies, the lower threshold of the iterative analysis was adjusted to 85% (see below).

Figure 6 depicts multi-echo FLASH results at  $0.3 \times 0.3 \times 1.5$  mm<sup>3</sup> or 0.135  $\mu$ L resolution. The top image represents the original correlation coefficient map without any thresholding. The two central images refer to statistically evaluated and color-coded activation maps superimposed on an averaged raw image. They were obtained by using either the standard thresholds as in Fig. 4 or an upper threshold of 99.99% in conjunction with a lower threshold of 85%. The rationale for this latter value becomes obvious by a direct comparison of the resulting activation map with the 'unbiased' correlation coefficient map. Whereas the standard thresholds optimized for a conventional number of image pixels clearly underestimate the extent of positive correlations visible in the correlation map, a lowered second threshold of 85% much better matches the number of truly activated pixels, although still in a conservative manner and without adding false-positive areas.

## DISCUSSION

Despite an increase of the resolution by a factor of 200 relative to conventional EPI studies performed at  $3 \times 3 \times 3$  mm<sup>3</sup> or 27  $\mu$ L voxel size, multi-echo FLASH activation maps reveal robust activations in primary visual areas and no false-positive voxels outside. It should be emphasized that the sequence did not result in more severe motion problems than are usually observed for studies at lower resolution. Corrupted data sets, which are easily detectable by visual inspection of the correlation coefficient maps, were discarded at a similar rate as for other studies in this laboratory. A highly desirable effect of high spatial resolution is the reduction of macroscopic susceptibility artifacts, which typically refer to magnetic field inhomogeneities that expand over dimensions of multiple voxels. Therefore, regardless of the fact that the intrinsic  $T_2^*$  attenuation of a multi-echo FLASH sequence is similar to that of a conventional single-shot EPI sequence, the pronounced decrease of artifactual intravoxel dephasing with decreasing voxel size effectively minimizes geometric distortions and signal losses experienced at lower resolution. On the other hand, acquisitions at ultra-high resolution certainly sacrifice SNR of the individual raw images. The correspondingly increased contribution from thermal noise makes it even more difficult to study subjects that may already be characterized as 'weak' BOLD MRI responders at conventional spatial resolution.

In principle, the in-plane resolution could be even further increased by reducing the FOV while keeping the acquisition matrix constant. For example, for studies

of the occipital cortex, the procedure would cause tolerable aliasing artifacts along the phase-encoding dimension of the image up to a resolution of about  $0.2 \times 0.2$  mm<sup>2</sup>. However, this approach was precluded by reaching the technical capabilities of the gradient power supply. Alternatively, the voxel size may also be decreased by reducing the section thickness to 1 mm or less. Thin sections with acceptable slice profile were accomplished by prolonging the pulse duration to 5.12 ms. Respective acquisitions yielded functional activation maps of similar quality as in Fig. 5 for an isotropic spatial resolution of  $0.5 \times 0.5 \times 0.5$  mm<sup>3</sup> or 0.125  $\mu$ L voxel size (not shown). However, any attempt to decrease the voxel size further resulted in insufficient contrast-to-noise for reliable BOLD MRI studies of the human brain. Hence, for the given hardware – and this particularly applies to the four-channel RF coil used – it must be concluded that the results shown represent the maximum spatial resolution for a functional MRI experiment with reasonable temporal resolution.

Finally, it is fair to say that – similarly to most other MRI acquisitions – the numbers given for the spatial resolution refer to what one may call *nominal* resolution. Whereas the in-plane pixel size is affected by  $T_2^*$  modulation of the  $k$ -space data yielding a broadening of the point-spread function along the phase-encoding dimension, the actual slice profile depends not only on the duration and shape of the applied RF pulse but also on the degree of  $T_1$  saturation.

## CONCLUSIONS

A method is presented for functional MRI of the human brain at 0.135  $\mu$ L voxel size for a (single) whole brain section. With a truly acquired in-plane resolution of only 300  $\mu$ m linear pixel dimension, that is, without interpolation, a section thickness of 1.5 mm resulted in robust activations in primary visual areas in response to binocular stimulation.

In general, the minimum voxel size is determined by (i) technical constraints due to the available gradient power, (ii) physiological limitations due to peripheral nerve stimulation (gradient slew rate) and (iii) a reasonable SNR and temporal resolution as required for reliable functional MRI. Using optimized bandwidths and RF coils matched to the area under investigation, multi-echo FLASH with echo train shifting emerges as a technical approach to reach the limits.

## REFERENCES

1. Ogawa S, Lee TM, Nayak AS, Glynn P. Oxygenation-sensitive contrast in magnetic resonance imaging of rodent brain at high magnetic fields. *Magn. Reson. Med.* 1990; **14**: 68–78.
2. Frahm J, Merboldt KD, Hänicke W. Functional MRI of human brain activation at high spatial resolution. *Magn. Reson. Med.* 1993; **29**: 139–144.

3. Hoogenraad FGC, Hofmann MBM, Pouwels PJW, Reichenbach JR, Rombouts SARB, Haacke EM. Sub-millimeter fMRI at 1.5 tesla: correlation of high resolution with low resolution measurements. *J. Magn. Reson. Imaging* 1999; **9**: 475–482.
4. Yacoub E, Duong TQ, Van De Moortele PF, Lindquist M, Adriany G, Kim SG, Ugurbil K, Hu X. Spin-echo fMRI in humans using high spatial resolutions and high magnetic fields. *Magn. Reson. Med.* 2003; **49**: 655–664.
5. Menon RS, Ogawa S, Strupp JP, Ugurbil K. Ocular dominance in human V1 demonstrated by functional magnetic resonance imaging. *J. Neurophysiol.* 1997; **77**: 2780–2787.
6. Dechent P, Frahm J. Direct mapping of ocular dominance columns in human primary visual cortex. *Neuroreport* 2000; **11**: 3247–3249.
7. Menon RS, Goodyear BG. Submillimeter functional localization in human striate cortex using BOLD contrast at 4 tesla: implications for the vascular point-spread function. *Magn. Reson. Med.* 1999; **41**: 230–235.
8. Goodyear BG, Menon RS. Brief visual stimulation allows mapping of ocular dominance in visual cortex using fMRI. *Hum. Brain Mapp.* 2001; **14**: 210–217.
9. Cheng K, Waggoner RA, Tanaka K. Human ocular dominance columns as revealed by high-field functional magnetic resonance imaging. *Neuron* 2001; **32**: 359–374.
10. Yacoub E, Ugurbil K, Shmuel A. Robust detection of ocular dominance columns in humans using high field HSE BOLD fMRI. *Proc. Int. Magn. Reson. Med.* 2004; **11**: 1054.
11. Feinberg DA, Oshio K. Gradient-echo shifting in fast MRI techniques (GRASE imaging) for correction of field inhomogeneity errors and chemical shift. *J. Magn. Reson.* 1992; **97**: 177–183.
12. Baudewig J, Dechent P, Merboldt KD, Frahm J. Thresholding in correlation analyses of magnetic resonance functional neuroimaging. *Magn. Reson. Imaging* 2003; **21**: 1121–1130.